than 3 eV is possible in the polymers that have a molecular weight of over 5000. Therefore, this is consistent with the observation of visible photoluminescence in these polymers. The broadness of the spectra are suggested to come from the variety of polymer sizes and dimensionality.

Conclusion

Silicon network polymers exhibit quite different optical properties from linear polysilanes. Their absorption spectra have completely different profiles, and they have broad photoluminescence spectra in the visible light region. These optical properties are attributed to a silicon network structure with a high dimensionality close to that of a 2D structure. These new materials provide important clues in bridging the gap between 1D and 3D silicon structures.

Acknowledgment. We express our thanks to Hiroshi Kojima and Hiroaki Isaka for contributing the experimental data used in this work.

References and Notes

(1) West, R. *J. Organomet. Chem.* **1986**, *300*, 327.
(2) Kagawa, T.; Fujino, M.; Takeda, K.; Matsumoto, N. *Solid State Commun.* **1986**, *57*, 635.
(3) Kepler, R. G.; Zeigler, J. M.; Harrah, L. A.; Kultz, S. R. *Phys. Rev. B* **1987**, *35*, 2818.
(4) Fujino, M. *Chem. Phys. Lett.* **1987**, *136*, 451.
(5) Kajzar, F.; Messier, J.; Rosilio, C. *J. Appl. Phys.* **1986**, *60*, 3040.
(6) Stolka, M.; Yuh, H. J.; McGrane, K.; Pai, D. M. *J. Polym. Sci., Part A: Polym. Chem.* **1987**, *25*, 823.
(7) Takeda, K.; Teramae, H.; Matsumoto, N. *J. Am. Chem. Soc.* **1986**, *108*, 8186.
(8) Takeda, K.; Shiraishi, K. *Phys. Rev. B* **1989**, *39*, 11028.
(9) Teramae, H.; Takeda, K. *J. Am. Chem. Soc.* **1989**, *111*, 1281.
(10) Miller, R. D.; Sooriyakumaran, R. *J. Polym. Sci., Part C: Polym. Lett.* **1987**, *25*, 321.
(11) Matsumoto, N.; Takeda, K.; Teramae, H.; Fujino, M. *Advances In Silicon Based Polymers*; American Chemical Society: Washington, DC, in press.
(12) Bianconi, P. A.; Weidman, T. W. *J. Am. Chem. Soc.* **1988**, *110*, 2342.
(13) Bianconi, P. A.; Schilling, F. C.; Weidman, T. W. *Macromolecules* **1989**, *22*, 1697.
(14) Details of the synthesis and structural analysis will be published in another paper.
(15) Schilling, F. C.; Bovey, F. A.; Zeigler, J. M. *Macromolecules* **1986**, *19*, 2309.
(16) These two absorption peaks are based on two different conformations in the dihexylpolysilane. Polysilanes that have a unique conformation exhibit only one peak.
(17) Polysilanes, such as dihexylpolysilane and methylphenylpolysilane, are also synthesized using crown ether as a cocatalyst to increase the yields. However, even in these polymers, no visible photoluminescence has ever been observed.
(18) Harrah, L. A.; Zeigler, J. M. *Macromolecules* **1987**, *20*, 601.
(19) Ito, O.; Terazima, M.; Azumi, T.; Matsumoto, N.; Takeda, K.; Fujino, M. *Macromolecules* **1989**, *22*, 1718.
(20) Matsumoto, N.; Furukawa, S.; Takeda, K. *Solid State Commun.* **1985**, *53*, 881.

Characterization of the Chain Dynamics of PEEK by CPMAS ^{13}C NMR

Mark D. Poliks and Jacob Schaefer*

Department of Chemistry, Washington University, St. Louis, Missouri 63130

Received November 6, 1989

ABSTRACT: Dipolar rotational spin-echo, $T_1(C)$, $T_{1\rho}(C)$, and both direct and indirect $T_{1\rho}(H)$ relaxation experiments have been performed on partially crystalline poly(oxy-1,4-phenyleneoxy-1,4-phenylenecarbonyl-1,4-phenylene), commonly known as PEEK. The results of these experiments demonstrate that main-chain aromatic rings are dynamically active in only a relatively small part of the amorphous fraction. Most of the rings in both amorphous and crystalline regions are immobile. On average, the ether-ether rings in the amorphous regions of PEEK are slightly less mobile than the ether-ketone rings, presumably the result of interchain packing in the lattice.

Introduction

Poly(oxy-1,4-phenyleneoxy-1,4-phenylenecarbonyl-1,4-phenylene), commonly known as PEEK,[1] has only ether oxygens and carbonyl carbons linking main-chain aromatic rings. PEEK is hydrophobic and resists all common organic solvents. Because PEEK can be heated above the melting point of its crystalline phase without chemical degradation, the fabrication of tough PEEK composites is practical. Gaining some understanding of the mechanical properties of these composites may be helped by a characterization of the microscopic chain dynamics of the PEEK matrix.

Magic-angle spinning, natural-abundance ^{13}C NMR experiments can be performed on samples of PEEK to be used in engineering applications. Special preparations of labeled materials are not required. Many of the natural-abundance ^{13}C NMR methods developed to characterize PEEK as a homopolymer can also be applied to PEEK as one component of an engineering composite. In this paper, we report the results of a variety of ^{13}C NMR dynamics experiments performed on partially crystalline samples of PEEK homopolymer. We interpret these results in terms of motions of the two kinds of main-chain aromatic rings of PEEK, in either the amorphous or crystalline regions of the polymer.

Experiments

Magic-Angle Spinning. Cross-polarization magic-angle spinning ^{13}C NMR spectra were obtained at room temperature on

0024-9297/90/2223-3426$02.50/0

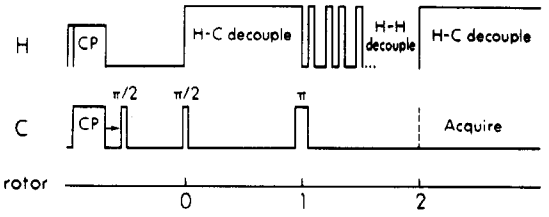

Figure 1. Pulse sequence for the measurement of spin-edited H–C dipolar evolution. The first delay time (arrow) was 60 μs.

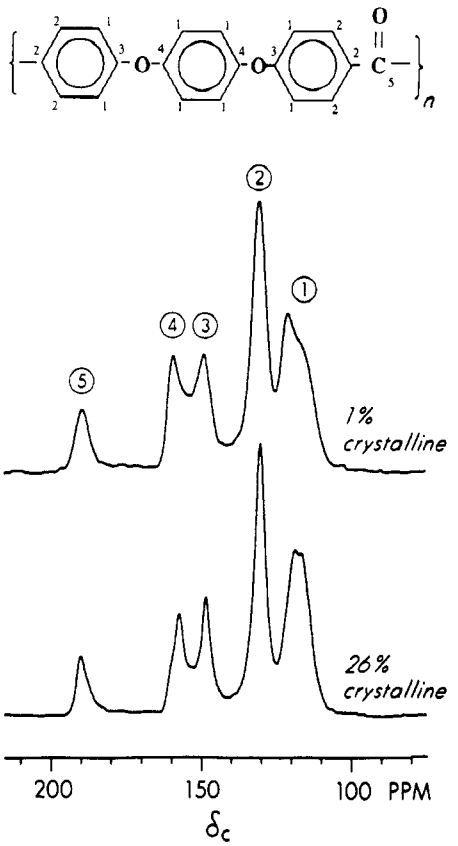

Figure 2. 15.1-MHz CPMAS ^{13}C NMR spectra of two partially crystalline PEEK's. The numbers in the structural formula of the repeat unit assign carbons to resonances.

a spectrometer built around a 12-in. iron magnet operating at a proton Larmor frequency of 60 MHz.[2] Contact times of 2.0 ms and repetition periods of 1 s were standard. Half-gram samples were spun in a double-bearing rotor[3] at 1859 or 930 Hz. The long-term stability of the spinning speed was ±1 Hz. $T_1(C)$ was measured by the Torchia method[4] and $T_{1\rho}(C)$ by standard procedures.[5]

Carbon Dipolar Sideband Patterns. Carbon dipolar line shapes were characterized by dipolar rotational spin–echo (DRSE) ^{13}C NMR. This is a two-dimensional experiment[6] in which, during the additional time dimension, carbon magnetization is allowed to evolve under the influence of H–C coupling while H–H coupling is suppressed by homonuclear multiple-pulse semiwindowless MREV-8 decoupling.[7] The cycle time for the homonuclear decoupling pulse sequence was 33.6 μs, resulting in decoupling of proton–proton interactions as large as 60 kHz. Sixteen MREV-8 cycles fit exactly in one rotor period so that strong dipolar echoes formed. A 16-point Fourier transform of the time dependence of the intensity of any peak resolved by magic-angle spinning in the chemical-shift dimension yielded a symmetrized 16-point dipolar spectrum, scaled by the MREV-8 decoupling and broken up into sidebands by the spinning.[8,9] Sideband ratios in symmetrized dipolar patterns are averages of those in unsymmetrized patterns.

Spin Editing. If a resolved peak arises from a combination of contributions from both protonated and nonprotonated carbons, the resultant DRSE sideband pattern will not be interpretable in a direct way. This situation occurs for PEEK. To remove the contributions from the protonated carbons and simplify the pattern, the dipolar evolution period was preceded by an H–C dephasing period in the presence of H–H coupling (Figure 1). This period was typically 60 μs and was followed by a flip-back pulse which restored the remaining carbon magnetization to the H_0 direction. Only magnetization from nonprotonated carbons survived the dephasing. A subsequent, longer delay allowed residual x–y magnetization resulting from pulse imperfections to disappear. The second delay could be chosen so that the time from the end of the CP contact to the start of the dipolar evolution was exactly one rotor period, a necessary precaution in other systems[10] where H–C coupling for protonated carbons is not much larger than chemical-shift anisotropy. The dipolar sideband pattern of the protonated carbons contributing to the combination line can then be determined by the difference of patterns obtained without and with dephasing spin editing.

In addition to spin editing by dephasing, DRSE patterns were sometimes altered by preceding the dipolar evolution with a variable-delay $T_1(C)$ waiting period to allow fast-relaxing components to escape.

Materials. Samples of PEEK of varying crystallinity were prepared in the McDonnell Douglas Research Laboratories by the quenching and annealing of bulk polymer obtained from Imperial Chemical Industries. Crystallinity was estimated from density (Table I). A sample of poly(oxy-1,4-phenylenecarbonyl-1,4-phenylene), commonly known as poly(ether ketone) or PEK, was prepared by quenching in ice water a 350 °C melt of material supplied by Imperial Chemical Industries (Victrex PEK, LKB-100).

Table I
Crystallinity of PEEK as a Function of Thermal History

thermal history	density, g/mL	crystallinity, %
as received[a]	1.2651	1.0
152 °C for 75 min	1.2658	2.5
153 °C for 75 min	1.2731	8.5
156 °C for 75 min	1.2852	18.0
as received[b]	1.2963	26.0

[a] ICI Victrex PEEK (K200). [b] ICI Victrex PEEK (XK300).

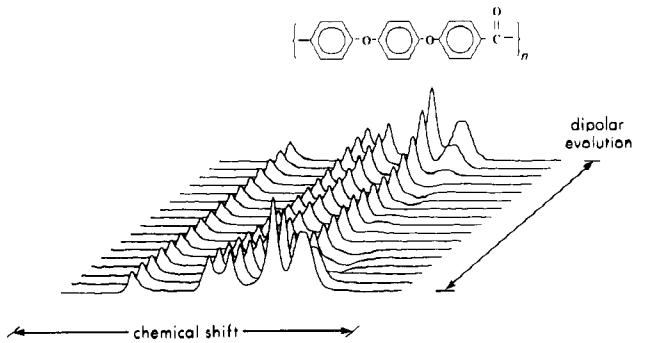

Figure 3. Dipolar evolution of a 26%-crystalline PEEK. The H–C dipolar evolution occurred over 536 μs (one rotor period) with H–H dipolar interactions removed by semiwindowless MREV-8 homonuclear decoupling.

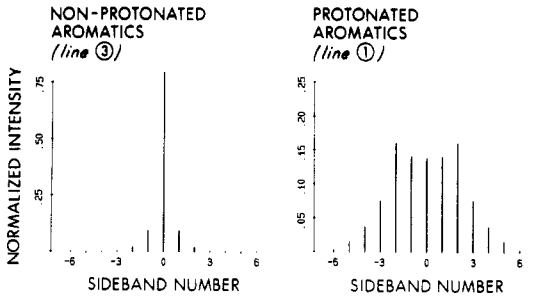

Figure 4. Fourier transforms of the dipolar evolution of the centers of two of the lines of Figure 3.

Table II
Dipolar Rotational Sideband Intensities[a] for the Center[b] of Line 1 of PEEK[c]

period, s	CP contact, ms	sideband no. 0	1	2	3	4	5
1	0.5	0.148	0.154	0.176	0.075	0.034	0.005
	2.0	0.151	0.154	0.178	0.077	0.032	0.005
4	0.5	0.150	0.154	0.178	0.077	0.035	0.006
	2.0	0.144	0.146	0.178	0.081	0.035	0.006

[a] Semiwindowless MREV-8 multipulse decoupling. Theoretical scale factor is 0.54. Magic-angle spinning at 1859 Hz. [b] Chemical shift of 117 ppm. [c] 26% crystalline.

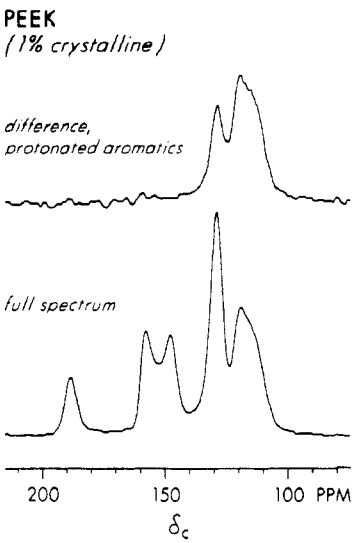

Figure 5. Dipolar echo spectra of a 1%-crystalline PEEK without dephasing spin editing preceding dipolar evolution (bottom) and the difference between with and without dephasing spin editing preceding dipolar evolution (top).

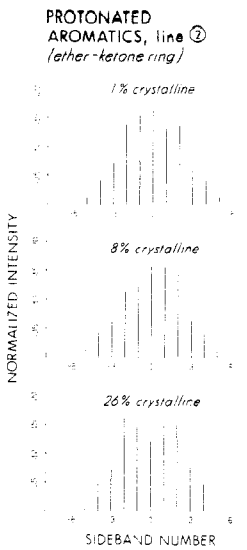

Figure 6. Dipolar sideband patterns for spin-edited line 2 of PEEK as a function of crystallinity.

Table III
Dipolar Rotational Sideband Intensities[a] for the Right Side[b] of Line 1 of PEEK[c] as a Function of Dephasing Spin Editing

spin editing	sideband no. 0	1	2	3	4	5
none	0.137	0.140	0.160	0.076	0.037	0.015
60-μs dephasing[d]	0.083	0.147	0.166	0.088	0.059	0.007

[a] Semiwindowless MREV-8 multiple-pulse decoupling. Theoretical scale factor is 0.54. Magic-angle spinning at 1859 Hz. [b] Chemical shift of 116 ppm. The center of the line is at 117 ppm. [c] 26% crystalline. [d] Sideband pattern obtained with no dephasing minus that obtained with dephasing (chemical shift 116 ppm).

Table IV
Dipolar Rotational Sideband Intensities[a] for Spin-Edited[b] Line 2 of PEEK

sample crystallinity, %	sideband no. 0	1	2	3	4	5
1	0.162	0.154	0.139	0.072	0.042	0.013
8	0.157	0.155	0.146	0.062	0.046	0.012
26	0.122	0.146	0.160	0.083	0.046	0.004

[a] Semiwindowless MREV-8 multiple-pulse decoupling. Theoretical scale factor is 0.54. Magic-angle spinning at 1859 Hz. [b] Sideband pattern obtained with no dephasing minus that obtained with 60-μs dephasing (see Figure 1).

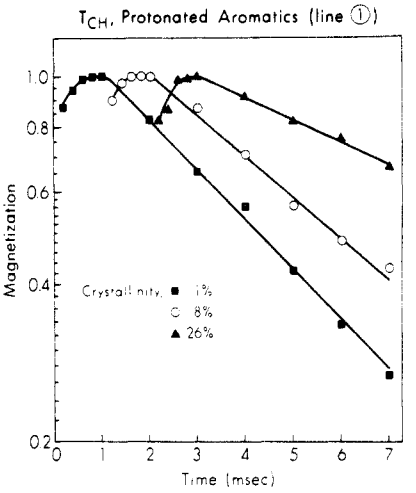

Figure 7. Matched spin-lock, ^1H–^{13}C cross-polarization transfer dynamics at 50 kHz for PEEK as a function of crystallinity.

Results

^{13}C NMR Spectra and Dipolar Evolution. Characterization of the chain dynamics of PEEK by natural-abundance ^{13}C NMR is complicated by the compactness of the aromatic-carbon region of the spectrum (Figure 2). In general, the most directly accessible ^{13}C NMR information about motion is obtained from protonated carbons. The protonated aromatic carbons of PEEK contribute to lines 1 and 2 at 117 and 127 ppm, respectively.[11] Line 1 arises from both the protonated aromatic carbons of the ether–ether and ether–ketone rings, while line 2 arises from both protonated and nonprotonated carbons of the ether–ketone rings. Thus, in the rotor-synchronized DRSE experiment, line 1 is totally dephased, but line 2 is only partially reduced in amplitude by dephasing (Figure 3). The remaining three lines of the PEEK spectrum, all arising exclusively from nonprotonated carbons, are not significantly reduced in amplitude by dephasing during the dipolar evolution period (Figure 3).

The Fourier transform of the dipolar evolution of the center of line 1 yields a dipolar sideband pattern (Figure 4, right) which indicates qualitatively an average ampli-

Table V
$T_{1\rho}$(H)[a] (ms) of PEEK from Cross-Polarization Transfer

line no.[b]	sample crystallinity 1%	8%	26%
1	4.3	5.6	10.0
2	4.1	5.2	8.6
3	3.7	5.0	8.6
4	3.9	4.6	8.8
5	5.4	4.8	8.6

[a] Radio-frequency field amplitude of 50 kHz. [b] Line assignments of Figure 2.

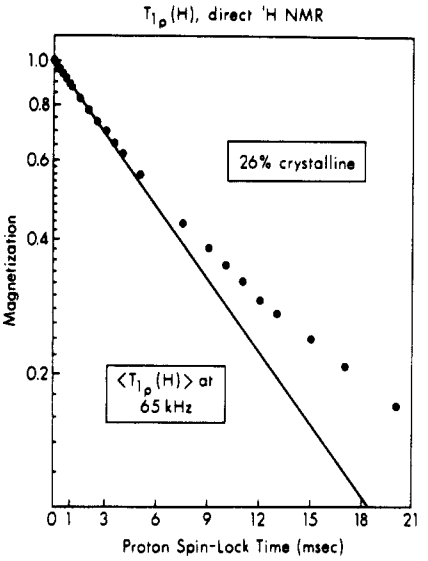

Figure 8. 60-MHz $T_{1\rho}$(H) decay for the protons of a 26%-crystalline PEEK. Proton magnetization was observed directly by a solid echo following a variable spin lock at 65 kHz.

Table VI
Protonated-Aromatic $\langle T_{1\rho}(C)\rangle$[a] (ms) of PEEK

H_1(C), kHz	sample crystallinity 1%	8%	26%
37	6.7	9.4	13
44	7.0	8.3	11
50	6.0	8.2	12
60	6.4	7.6	12

[a] Least-squares fit to the observed decay between 0.05 and 1.00 ms after the turnoff of H_1(C).

tude of ring rotation less than that of, say, polycarbonate but more than that of polystyrene or poly(ethylene terephthalate).[8] The dipolar patterns of Figure 4 represent contributions from all the carbons in PEEK. Conditions for the cross-polarization preparation part of the DRSE experiment were selected so that discrimination between crystalline and amorphous phases did not occur. The PEEK sideband patterns for line 1, for example, are the same for cross-polarization preparation contact times of 0.5 and 2.0 ms and for experiment repetition periods of 1 and 4 s (Table II).

Difference Spectra and Dipolar Patterns for the Ether–Ketone Rings. The dipolar spectrum of line 2 arises just from the ether–ketone rings but is complicated by an intense centerband (and measurable first sideband, Figure 4, left) from the nonprotonated carbons of the ether–ketone rings. These contributions can be removed by spin editing preceding the dipolar evolution (Figure 1). The nonprotonated aromatic-carbon magnetization is essentially unaffected by the 60-μs editing and so disappears from the difference between spectra obtained with and without spin editing. On the other hand, the protonated aromatic-carbon magnetization is totally

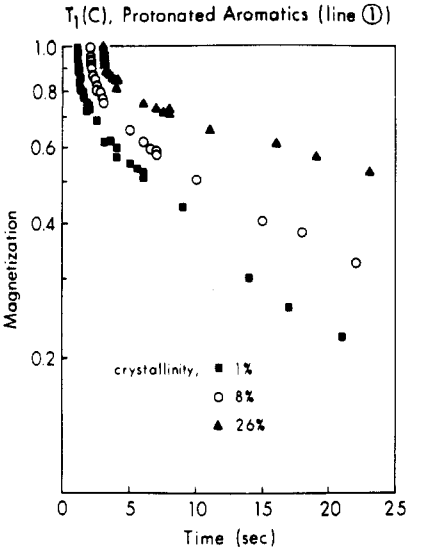

Figure 9. 15.1-MHz T_1(C) decay for the protonated aromatic carbons of PEEK as a function of crystallinity.

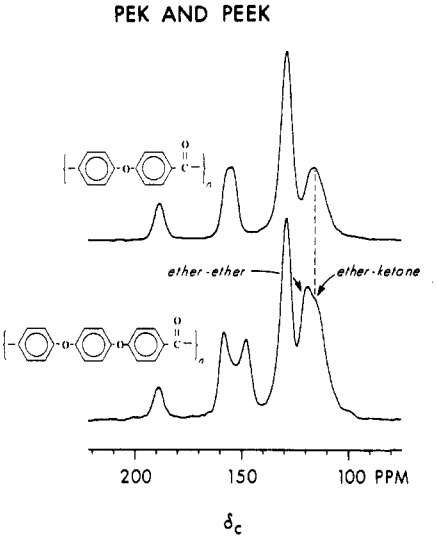

Figure 10. 15.1-MHz CPMAS ^{13}C NMR spectra of poly(ether ketone) (top) and poly(ether ether–ketone) (bottom).

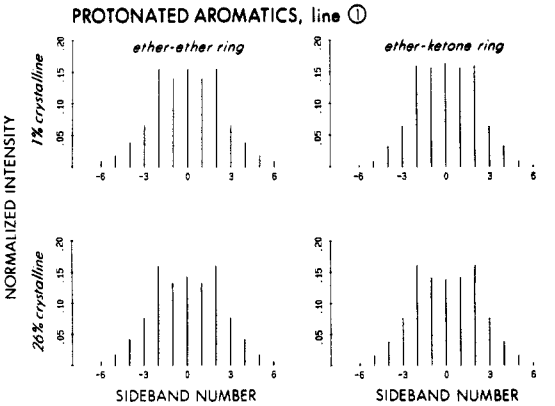

Figure 11. Dipolar sideband patterns for line 1 of PEEK as a function of crystallinity. The patterns on the left-hand side of the figure were obtained by using a chemical shift 1 ppm to the left of center of line 1, and those on the right-hand side of the figure were obtained from a chemical shift 1 ppm shift to the right of center.

dephased by the editing and so appears unchanged in the difference spectrum (Figure 5).

Except for the centerband, the protonated-carbon dipolar patterns are not affected by the dephasing spin editing. For example, the ratio of the second to first dipolar

Table VII
Dipolar Rotational Sideband Intensities[a] for the Center of Line 1 of PEEK[b] as a Function of T_1(C) Spin Editing

expt or calculation	sideband no. 0	1	2	3	4	5
full echo, no T_1(C) delay	0.151	0.154	0.178	0.077	0.032	0.005
4-s T_1(C) delay	0.112	0.131	0.184	0.091	0.043	0.017
difference, normalized	0.269	0.224	0.161	0.035		
calc,[c] π flips	0.238	0.238	0.104	0.031	0.007	
calc,[c] flips, oscillations, wiggles	0.273	0.239	0.094	0.025	0.005	
calc,[c] static	0.124	0.133	0.185	0.070	0.034	0.012

[a] Semiwindowless MREV-8 multiple-pulse decoupling. Theoretical scale factor is 0.54. Magic-angle spinning at 1859 Hz. [b] 26% crystalline. [c] Effective scale factor is 0.39. Details of the calculation are described in refs 8 and 9.

Table VIII
Experimental and Calculated Dipolar Rotational Sideband Intensity Ratios for Protonated Carbons of Ether–Ether and Ether–Ketone Rings of PEEK

sample crystallinity, %	n_2/n_1 ether–ether[a] exp	calc	ether–ketone[b] exp	calc
1	1.12	1.12[c]	1.03	1.00[d]
26	1.21	1.19[e]	1.14	1.19[e]

[a] 118-ppm left-hand dipolar slice of line 1; center of line is at 117 ppm. [b] 116-ppm right-hand dipolar slice of line 1; center of line is at 117 ppm. [c] 85% static plus 15% π flips superimposed on 20° oscillations. [d] 75% static plus 25% π flips superimposed on 10° oscillations. [e] 90% static plus 10% π flips superimposed on 10° oscillations.

sidebands (n_2/n_1) for the right-hand side of combination line 1 for the 26%-crystallinity sample is 1.13 with, and 1.14 without, dephasing spin editing (Table III). This means that the dipolar difference spectrum for spin-edited line 2 can be used to characterize unambiguously the amplitude of motion of just the ether–ketone ring. The n_2/n_1 sideband ratio for spin-edited line 2 increases with crystallinity (Table IV and Figure 6).

Rotating-Frame and Laboratory Spin–Lattice Relaxation. Proton $T_{1\rho}$'s increase with higher PEEK crystallinity as measured either indirectly by a cross-polarization transfer to carbons (Figure 7 and Table V) or directly by means of a ^{1}H spin-locking radio-frequency field. Results of the two experiments are in agreement. In the latter experiment, two-phase behavior is apparent for samples of higher crystallinity from multiple-component relaxation over long spin-lock times (Figure 8).

The protonated aromatic-carbon $T_{1\rho}$ is independent of applied H_1(C) but is sensitive to sample crystallinity (Table VI). The protonated aromatic-carbon T_1 is also sensitive to crystallinity (Figure 9). The 1%-crystalline PEEK has 20–40% of its protonated aromatic carbons with a short T_1(C), while the 26%-crystalline material has 10–20% fast relaxers. The dipolar sideband patterns for these slow- and fast-relaxing components are markedly different (Table VII, rows 2 and 3, respectively).

Discussion

Main-Chain Motion in Amorphous and Crystalline Domains. The fast-relaxing T_1(C) component in the 26%-crystalline sample of Figure 9 arises from aromatic carbons whose dipolar pattern matches that for rings undergoing 180° flips superimposed on small-amplitude ring oscillations and wiggles (Table VII, rows 3 and 5). However, this fraction represents only 10–20% of the total (Figure 9, solid triangles). The remainder (which includes all of the crystalline fraction) is essentially immobile (Table VII, rows 2 and 6). This result means that main-chain rings in most of the amorphous regions of PEEK are immobile. This conclusion is consistent with the moderately broad DRSE pattern observed for the 99%-amorphous sample (Figure 6, top). As crystallinity increases, the fraction of mobile rings decreases and the total dipolar sideband pattern broadens (Figure 6, bottom). On the basis of the short average T_1(C) and the H_1(C) independence of $T_{1\rho}$(C), the average frequency of flips, oscillations, and wiggles is between 100 kHz and 1 MHz. Because chains with immobile rings comprise the more slowly relaxing components in both T_1(C) and $T_{1\rho}$(C) experiments, the average values of these relaxation parameters increase with higher crystallinity (Figure 9 and Table VI).

Ether–Ketone and Ether–Ether Ring Mobilities. For the 26%-crystalline PEEK, comparison of the dipolar pattern of the center of combination line 1 (Figure 4, right, and Table VII, row 1) with the dipolar pattern of the ether–ketone protonated aromatic carbons of spin-edited line 2 (Figure 6, bottom, and Table IV, row 3) shows that the n_2/n_1 ratio is slightly larger for the center of combination line 1 (1.16 for the combination line, compared to 1.10 for the ether–ketone carbon line). The 5% difference is outside the 2% experimental variability in n_2/n_1. This means that n_2/n_1 ratios are greater (and so the dipolar patterns wider) for the ether–ether rings than for the ether–ketone rings.

We reach the same conclusion about n_2/n_1 ratios more directly by examining multiple dipolar sideband patterns from line 1 alone. This approach avoids dephasing spin editing. The low-field side of combination line 1 (118 ppm) arises predominantly from ether–ether protonated carbons, while the high-field side (116 ppm) arises predominantly from ether–ketone protonated carbons. These assignments are based on the spectrum of poly(ether ketone), which has no contributions from ether–ether rings (Figure 10). Then, from dipolar slices to the low- and high-field sides of the center of line 1, we see that the n_2/n_1 ratio is slightly greater for the ether–ether ring than for the ether–ketone ring for both low- and high-crystalline-content samples (Figure 11).

If the n_2/n_1 ratio is greater for the ether–ether rings than for the ether–ketone rings, then, on average, the ether–ether rings are less mobile than the ether–ketone rings. The difference in mobility may be due either to fewer ether–ether rings than ether–ketone rings undergoing 180° flips in the amorphous regions or to slightly smaller amplitude oscillations and wiggles for the ether–ether rings (Table VIII). However, intuition based on isolated-chain intramolecular steric interactions dictates that ether–carbon linkages are more flexible than carbonyl–carbon linkages. We therefore attribute the experimental observation of reduced mobility of the ether–ether rings to the influence of interchain packing in the amorphous PEEK lattice.

Acknowledgment. This work was conducted under the McDonnell Douglas Research Laboratories (St. Louis) Independent Research and Development Program.

References and Notes

(1) The Imperial Chemical Industries trademark is Victrex PEEK.
(2) Schaefer, J.; Stejskal, E. O. *Top. Carbon-13 NMR Spectrosc.* **1979**, *3*, 284.
(3) Schaefer, J.; Garbow, J. R.; Stejskal, E. O.; Lefelar, J. A. *Macromolecules* **1987**, *20*, 1271.
(4) Torchia, D. A. *J. Magn. Reson.* **1978**, *30*, 613.
(5) Schaefer, J.; Sefcik, M. D.; Stejskal, E. O.; McKay, R. A. *Macromolecules* **1984**, *17*, 1118.
(6) Munowitz, M. G.; Griffin, R. G. *J. Chem. Phys.* **1982**, *76*, 2848.
(7) Burum, D. P.; Linder, M.; Ernst, R. R. *J. Magn. Reson.* **1981**, *44*, 173.
(8) Schaefer, J.; Stejskal, E. O.; McKay, R. A.; Dixon, W. T. *Macromolecules* **1984**, *17*, 1479.
(9) Garbow, J. R.; Schaefer, J. *Macromolecules* **1987**, *20*, 819.
(10) Poliks, M. D.; Schaefer, J. *Macromolecules* **1990**, *23*, 2682.
(11) Clark, J. N.; Jagannathan, R. R.; Herring, F. G. *Polymer* **1988**, *29*, 341.

Registry No. PEEK, 31694-16-3.

Two-Dimensional Solid-State NMR Studies of Ultraslow Chain Motion: Glass Transition in Atactic Poly(propylene) versus Helical Jumps in Isotactic Poly(propylene)

D. Schaefer and H. W. Spiess*

Max-Planck-Institut für Polymerforschung, Postfach 3148, D-6550 Mainz, West Germany

U. W. Suter

Institut für Polymere, ETH Zentrum, CH-8092 Zürich, Switzerland

W. W. Fleming

Almaden Research Center, IBM Research Division, 650 Harry Road, San Jose, California 95120-6099

Received December 5, 1989

ABSTRACT: The deuteron 2D exchange experiment has been applied to study the ultraslow rotational chain dynamics of atactic (aPP) and isotactic poly(propylene) (iPP). The motional mechanism was found to be vastly different for these polymers, reflecting the different chain conformation and packing. Whereas in amorphous aPP in the vicinity of the glass transition a diffusive motion was observed, iPP was shown to perform helical jumps about the helix axis in the crystalline domains at temperatures above 360 K. The temperature variation of the mean correlation times, obtained from an analysis of the aPP spectra based on isotropic rotational diffusion with a distribution of correlation times, follows the WLF equation over 11 orders of magnitude between 10^{-10} and 10 s. The parameters extracted from this fit correspond to textbook values known from macroscopic measurements of the viscoelastic behavior in amorphous polymers. This shows that 2D NMR, although monitoring the chain dynamics via a localized probe, is able to follow the collective dynamics of the glass process. The discrete jump motion observed for iPP is caused by 120° rotations of the 3_1 helix about the helix axis. The relative angle of 113° between the methyl groups before and after the jump is determined from the 2D spectra directly without the need of interfacing a model and agrees with the value calculated from crystallographic data.

Introduction

The macroscopic properties of polymeric materials are often supposed to be governed by the molecular motion of the macromolecular chains.[1,2] The dynamics, in turn, depends on the arrangement of the chains in amorphous or crystalline states. A variety of physicochemical techniques have amply demonstrated the existence of several relaxations in completely amorphous as well as in partially crystalline polymers, and many studies are engaged in elucidating the molecular nature of these relaxations.[1,3,4] Among these techniques pulsed ^2H NMR and ^{13}C NMR have proved to be successful in probing molecular reorientations.[5-8] Most techniques, however, cannot clearly discriminate between different motional mechanisms proposed for polymer chain dynamics. The application of two-dimensional (2D) Fourier transform (FT) methods to the study of molecular motions[9] represents a major step in order to solve this problem: through the 2D exchange experiment the molecular orientation is measured via the NMR frequency *before* and *after* a mixing time t_m during which slow dynamic processes changing the molecular orientation may occur. Therefore, by systematic variation of t_m, the dynamic process can be followed in *real time*. Moreover, the experiment also yields unique geometric information since the angle by which the molecules rotate is measured directly, without the need of interfacing a model.[9,10]

In fact, each 2D exchange NMR spectrum represents a statistically well-defined two-time distribution function.[11] It describes the joint probability density to find molecules with NMR frequencies ω_1 before and ω_2 after the

0024-9297/90/2223-3431$02.50/0